ELSEVIER

Journal of Nuclear Materials 258–263 (1998) 1307–1311

journal of nuclear materials

Modelling of phase transformations occurring in low activation martensitic steels

J.-C. Brachet [a,*], L. Gavard [a], C. Boussidan [a], C. Lepoittevin [a], S. Denis [b], C. Servant [c]

[a] *Commissariat à l'Energie Atomique – Saclay, SRMA, Metallurgical Research Laboratory, 91191 Gif-sur-Yvette, France*
[b] *Ecole des Mines de Nancy, LSG2M, Parc de Saurupt 54042 Nancy, France*
[c] *Laboratoire de Métallurgie Struct., URA 1107, Université de Paris-Sud, 91405 Orsay, France*

Abstract

The main objective of this paper is to summarize modelling of on-heating and on-cooling phase transformations occurring in Low Activation Martensitic (LAM) steels. Calculations of thermodynamic equilibrium phase fractions and kinetic aspects of phase transformations have been performed by using different approaches from experimental data (CCT and TTT diagrams obtained by dilatometry). All the calculated data have been compared to an important and systematic set of experimental data obtained on different LAM steels of the 7.5–11% CrWVT a type.

1. Introduction

Low Activation Martensitic (LAM) steels are widely studied for Fusion Technology project as candidates for the first wall of Tokamaks. It is of technological interest to be able to predict the microstructural evolutions of LAM steels as a function of complex thermal cycles which can occur during fabrication, welding operations or in-service accidental conditions. So, this paper is especially focussed on the isothermal and anisothermal phase transformations that occur under heating and/or cooling for heating-cooling rates ranging from quasi-equilibrium conditions (i.e. ~0.01°C/s) up to dynamic conditions (i.e. ~100°C/s).

For this purpose, a series of six experimental heats, developed and supplied by AEA-Culham, and two large-scale heats (F82H and JLF1 from respectively JAERI and Tokyo University) have been considered in the present study.

2. Materials

The chemical composition of the selected heats is given in [1]. Schematically, the different alloys studied can be summarized as follows:

- 9%Cr–0.8W–V–(Ta) type: LA12LC, LA12TaLC and LA12TaLN;
- 7.5%Cr/9%Cr–2W–V–Ta: F82H and JLF1;
- 9%Cr–3%W–V–Ta: LA13Ta;
- 11%Cr–0.8W–V–Ta: LA4Ta.

Remark: 'LC' and 'LN' mean 'Low Carbon' and 'Low Nitrogen' respectively.

3. Experimental

All the martensitic samples were annealed at 1050°C for 30 min and quenched to room temperature to obtain the same initial metallurgical conditions. Then, the isothermal and anisothermal on-heating and on-cooling phase transformations were investigated using dilatometric facilities with heating/cooling rates ranging from 0.01°C/s up to 100°C/s. The main experimental results obtained in the present study are described in [1].

4. Modelling of phase transformations

4.1. Equilibrium conditions

Our first concern was to derive the equilibrium temperature of the ferrite $\Longleftrightarrow$ austenite phase transformation from data obtained in non-equilibrium

* Corresponding author. Tel.: +33 1 69 08 56 16; fax: +33 169 087 130; e-mail: jean-christophe.brachet@cea.fr.

0022-3115/98/$19.00
PII: S0022-3115(98)00197-4

conditions during heating. For this purpose, we have used the extrapolation relation derived by Zhu and Devletian [2]. From the classical heterogeneous nucleation theory, they have proposed the following relation to extrapolate the experimental data in equilibrium conditions:

$$T_s = C\left[S\,T_s \exp\left(\frac{E}{RT_s}\right)\right]^{1/3} + T_0, \qquad (1)$$

where T_s is the experimental temperatures measured at different heating/cooling rates, S, the heating/cooling rate, E the activation energy for intergranular or interphase diffusion. C a constant, T_0 the Equilibrium temperature.

In the present study, calculation of equilibrium temperatures was made using experimental data determined on heating with different rates and activation energies ranging from 80 to 400 kJ/mol. The choice of activation energy ranges corresponds to available data on diffusion activation energy for the main substitutional elements found in these materials. Table 1 summarizes all the typical equilibrium phase transformation temperatures derived from the Zhu and Devletian model from experimental on-heating data. Due to the activation energy range considered, the accuracy of the prediction seems to be close to +/−5°C.

On the other hand, to fully describe the different phases in equilibrium conditions, including minor precipitation, one can use thermodynamic approach with the help of 'Thermocalc' software associated with the 'Scientific Group Thermodata Europe' (SGTE)-Solution database [3]. From the minimization of Gibbs energy of the system, it is possible to compute all the possible equilibrium phases as a function of the temperature. The only input data are the chemical composition of the alloys. Fig. 1 compares $A_{10\%}$ and $A_{90\%}$ temperatures in equilibrium conditions extrapolated from experimental on-heating data using Eq. (1) with the values predicted by 'Thermocalc'. Taking into account the accuracy of the temperature measurements and of the extrapolation, the prediction seems to be quite good for $A_{90\%}$ temperature but the predicted $A_{10\%}$ temperature values are systematically lower than the experimental ones. Now, it is interesting to focus on the precipitated minor phases such as carbides, nitrides and intermetallic phases. For this class of steels, the major precipitated phase is the Chromium rich $M_{23}C_6$ carbide for temperatures corresponding to the conventional tempering conditions (that is 700–800°C). Complementary microstructural examinations have been performed to quantify and to analyse the precipitated minor phases of some of the alloys

Table 1
Equilibrium phase transformation temperatures extrapolated from on-heating experimental data using Eq. (1).

+/−5°C	A_s(°C)	$A_{10\%}$ (°C)	$A_{50\%}$ (°C)	$A_{90\%}$ (°C)	A_f(°C)
LA12TaLN	807	816	823	844	870
LA12LC	801	811	820	840	870
LA12Ta	804	813	822	838	862
LA13Ta	826	836	844	855	875
LA4Ta	839	844	850	860	896
F82H	840	843	845	867	902
JLF1	827	829	831	853	896

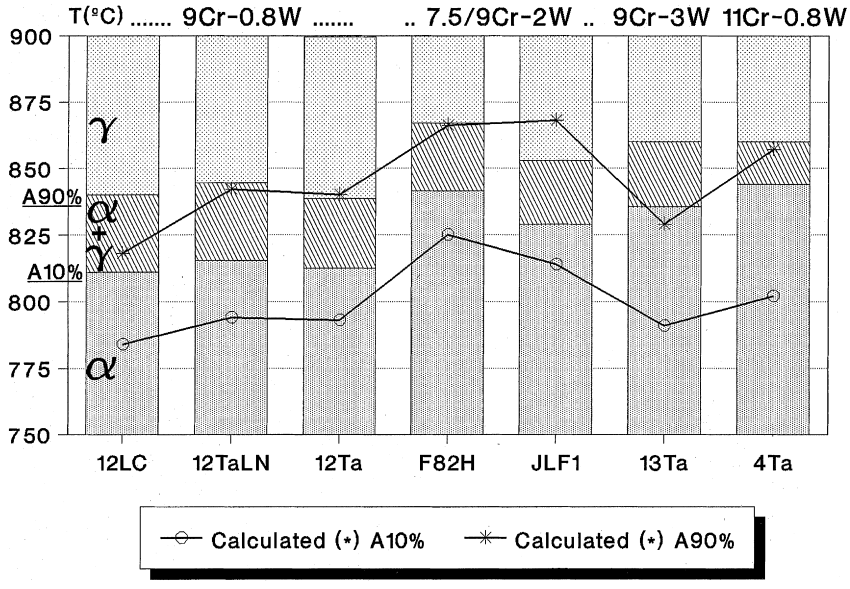

Fig. 1. Comparison between equilibrium phase temperatures $A_{10\%}$ and $A_{90\%}$ extrapolated from on-heating dilatometric results using Eq. (1) and predicted by 'Thermocalc'(*).

studied. Transmission Electron Microscopy (TEM) examinations using Electron Dispersive Energy (EDS) analysis have been performed on carbon extractive replica to determine the crystallographic structure and the chemical composition of the minor precipitates. Moreover, anodic dissolution of the matrix has allowed to quantify the full precipitated fraction. Fig. 2 shows the results obtained on F82H steel after tempering for 1 h at 700°C. From this figure, it should be noticed that both the chemical composition and the precipitated fraction of $M_{23}C_6$ carbide is consistent with 'Thermocalc' predictions.

4.2. Kinetic behaviour

An attempt has been made to predict the kinetic of anisothermal phase transformations for complex non linear heating-cooling thermal treatments. A first approach has consisted to use 'Phase RC' model developed by the LSG2M laboratory of the "Ecole des Mines de Nancy" [4]. This model is based on the principle of additivity. Calculations of the incubation period and the phase growth are performed separately. The heating/cooling thermal law is discretised in a succession of isothermal steps using the experimental kinetics of isothermal phase transformations. The incubation period (corresponding to start temperature: T_s) is determined according to Scheil's method [5], which assumes the additivity of incubation times (t_i) for each temperature:

$$\sum_{i=1}^{T_s} \frac{\Delta t_i}{t_i} = 1. \tag{2}$$

On cooling, the martensitic transformation is represented by the empirical relation of Koistinen–Marburger, which correlates the fractions of martensite (Y_m) and the residual austenite (not transformed into ferrite) fraction (Y_γ), the temperature (T) and the martensite start temperature (M_s) [6]:

$$Y_m = Y_\gamma(1 - \exp(-K\,(M_s - T))). \tag{3}$$

A second approach consisted in the use of a differential equation from Holt [7], slightly modified by introducing a supplementary term (1-y):

$$\frac{dy}{dt} = +/- K \exp\left(-\frac{E}{RT}\right)|T_{eq} - T|^m (1 - y) \tag{4}$$

where dy/dt is the instantaneous phase transformation rate, E an apparent activation energy for diffusion, T_{eq} the equilibrium temperature corresponding to the transformed phase fraction, y.

This model is related to a diffusion controlled phase transformation mechanism and so, cannot be used for on-cooling austenite $\Longleftrightarrow$ martensite transformation. On the other hand, the model is not able to predict accurately the 'incubation' period and must be used in conjunction with Scheil's method for example. The three adjustable constants are: K, E and exponent m, and have to be fitted on a series of experimental data obtained for different heating–cooling rates. Then, Eq. (4) can be integrated for any given thermal cycles to obtain the transformed phase fraction as a function of time and temperature.

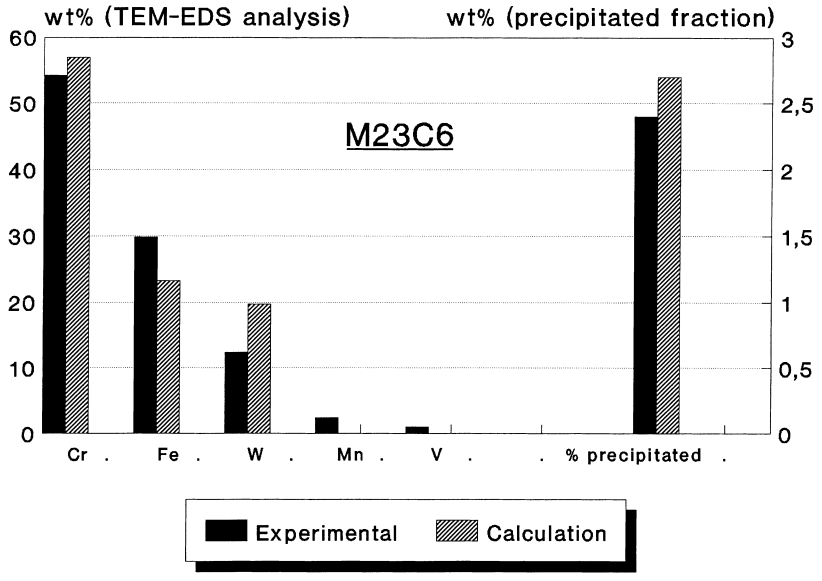

Fig. 2. Comparison between experimental results obtained by TEM-EDS analysis on carbon replica, anodic dissolution and predictions from 'Thermocalc' calculations, for the precipitation of M23C6 in F82H steel, after tempering for 1 h at 700°C.

4.3. On-heating {martensite and/or ferrite}⇒{austenite} transformation kinetics

Fig. 3 shows the typical transformation temperatures $A_{10\%}$, $A_{50\%}$ and $A_{90\%}$ corresponding to 10%, 50% and 90% of martensite transformed into austenite as a function of the heating rate for LA13Ta steel. The comparison of experimental values with the calculated ones using first approach presents a quite good agreement. Now, Fig. 4 compares the same experimental data with those calculated by integration of Eq. (4) with the following values for the constants:

$$K = 9.43 \times 10^{16}\, s^{-1}, \quad E = 472\ \text{kJ/mol}, \quad m = 2.$$

The experimental and calculated results show a good agreement.

4.4. On-cooling {austenite}⇒{martensite and/or ferrite} transformation kinetics

Under cooling, experimental CCT diagrams show that M_s temperature increases significantly when decreasing the cooling rate in the two-phased field [1]. This trend has already been explained in terms of a fast decrease of the interstitial atoms content (C and N) within the austenitic solid solution during the ferritic phase growth [8]. To take into account this unusual mecha-

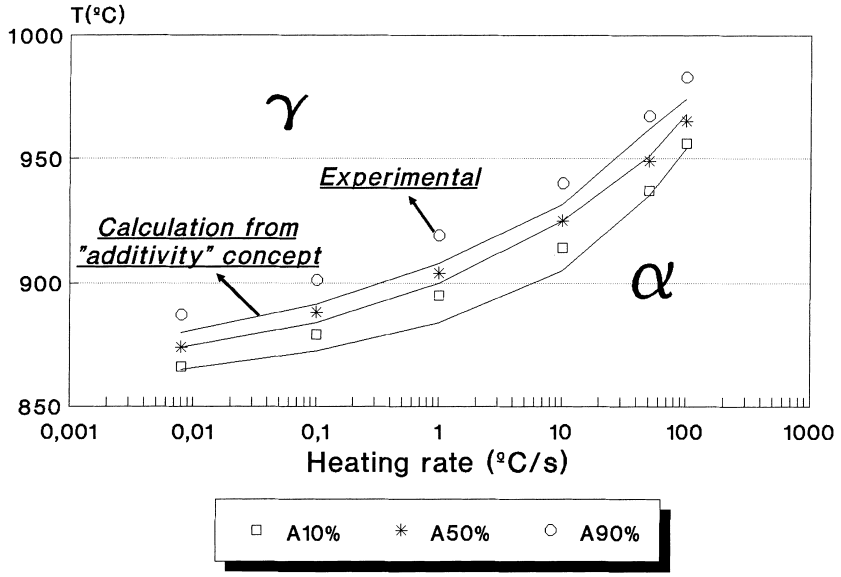

Fig. 3. Comparison between experimental and calculated (from 'additivity' concept) typical $\alpha \Rightarrow \gamma$ transformation temperatures as a function of the heating rate for the LA13Ta steel.

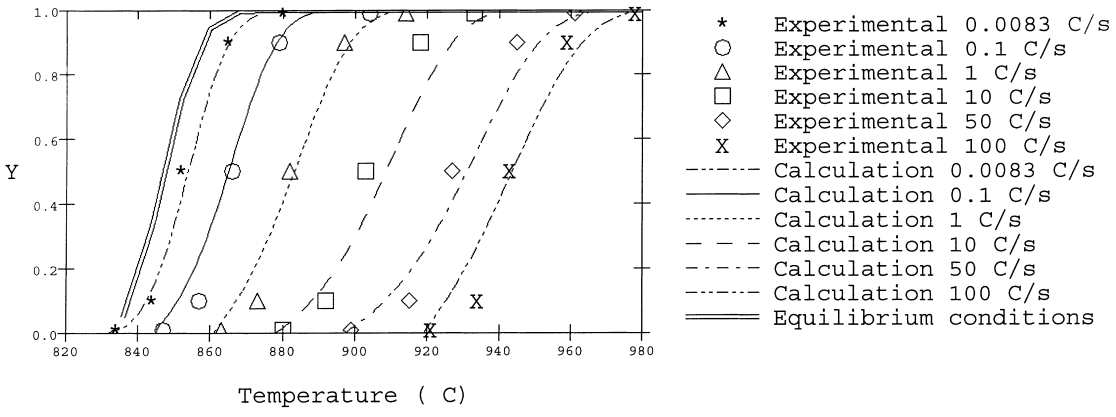

Fig. 4. Comparison between experimental and calculated (using integration of Eq. (4) on-heating $\alpha \Rightarrow \gamma$ transformation kinetics for LA13Ta steel.

nism, one can make the assumption that, in a first approximation, the observed M_s increase is controlled by diffusion of carbon (and/or nitrogen) in the parent austenitic phase. Then, from the kinetic point of view, the M_s increase must be related to the time (t) following a relation of the type:

$$\Delta M_s = \sqrt{Dt} \tag{5}$$

where D is the diffusion coefficient of C in the austenite.

Fig. 5 shows the evolution of M_s for cooling rates ranging from 25°C/h up to 400°C/h as a function of the inverse of the cooling rate. It is clear from this figure that the M_s evolution can be simply predicted by using Eq. (5). Thus, calculation of the full CCT diagram is obtained from additivity concept using the experimental TTT diagram as input and taking into account the M_s increase. The calculated results compare quite well with the experimental ones, as shown in Fig. 6 for La13Ta steel.

In some case (for LA12TaLN steel as an example), significant differences between calculated and experimental values are obtained on-cooling, where the calculated kinetics are much slower. This discrepancy could be due to the "non-additivity" of the incubation period. In this particular case, one can assume that some precipitation occurs on-cooling before the nucleation and growth of the ferrite (hyper-eutectoid behaviour) and further accelerates the anisothermal transformation.

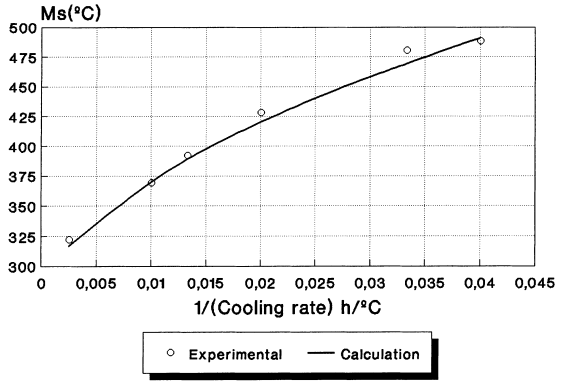

Fig. 5. Increase of M_s temperature as a function of the inverse of the cooling rate for LA13Ta steel and for cooling rates ranging from 25°C/h up to 400°C/h. Calculated curve corresponds to Eq. (5).

References

[1] A. Alamo, J.-C. Brachet, A. Castaing, C. Lepoittevin, F. Barcelo, these Proceedings.
[2] Y.T. Zhu, J.H. Devletian, Met. Trans. 22A (1991) 1993.
[3] B. Sundman, B. Jansson, J.O. Anderson, Calphad 2 (9) (1985) 153.
[4] F. Fernandes, S. Denis, A. Simon, Mem. Etud. Sci., Rev. Métall. (1986) 355.
[5] E. Sheil, Arch. Eisenhüttenwes. 8 (1935) 565.
[6] D.P. Koistinen, R.E. Marburger, Acta Metall. 7(1) (1959).
[7] R.A. Holt et al., IAEA Specialists meeting, IWGFPT/7, Blackpool, UK, 1980.
[8] J.-C. Brachet, Correlation between Thermoelectric Power and Martensite Start Temperature Measurements of 9Cr–W–V–Ta martensitic Steels, J. Phys. IV 5 (1995) C8-339.

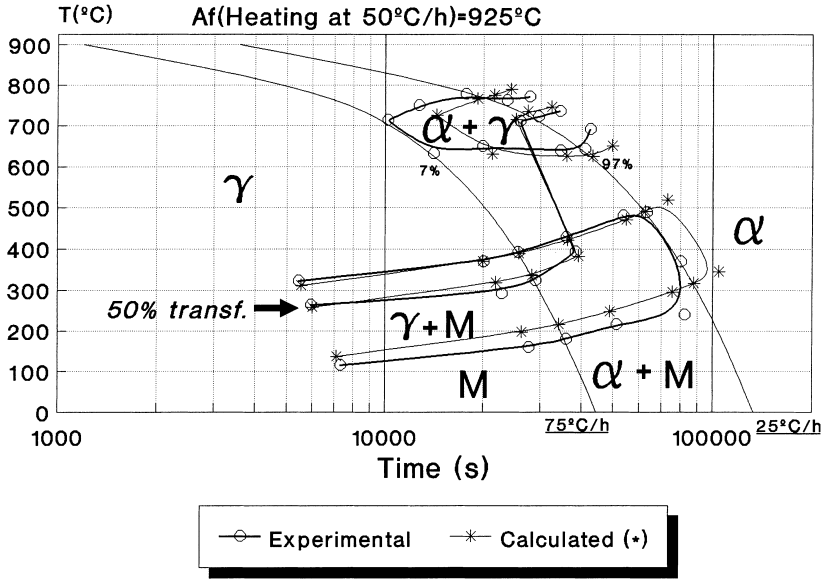

Fig. 6. Experimental and calculated CCT diagram of LA13Ta steel.